J. Micromech. Microeng. **10** (2000) 93–99. Printed in the UK PII: S0960-1317(00)09813-2

Rib-reinforced micromachined beam and its applications

Hung-Yi Lin and Weileun Fang

Power Mechanical Engineering Department, National Tsing Hwa University, Hsinchu, Taiwan

Received 24 November 1999

Abstract. The stiffness of a micromachined beam is usually restricted to the thickness of the thin-film materials. In this research, the rib-reinforced beam is proposed to increase the bending stiffness of thin-film micromachined structures. The increase of the bending stiffness of micromachined cantilevers has been demonstrated through analytical and experimental approaches. The fabrication processes required for the structure are compatible with the standard bulk micromachining processes. The primary contribution of the proposed design is that it can remarkably increase the bending stiffness of the micromachined structure without changing the thickness of the films. Hence, the design of the micromachined structure becomes more flexible. In application of the rib-reinforced structure, a micromachined lever mechanism is also designed and fabricated.

1. Introduction

The stiffness of micromachined structures is usually limited by the thickness of thin-film materials. Due to the existing of thin-film residual stresses, the micromachined structures could be remarkably deformed. For instance, a bending deformation of the micromachined cantilever could be produced by the gradient residual stress [1]. The micromachined bridge structure will buckle when it is under a uniform compressive residual stress [2]. Moreover, a significant deformation of the micromachined structure could attribute to external loads. For instance, the suspension of a torsional mirror is deformed by the electrostatic force in [3]. In [4], the mirror plate of an micromachined optical scanner is deflected by the inertia force.

At present, two techniques have been developed to reduce the deformation of the micromachined structures induced by the residual stresses. The first approach is to minimize the thin-film residual stresses by either optimizing the thin-film deposition conditions or using heat treatments after deposition [5, 6]. The second approach is to compensate the net bending moment induced by the residual stresses using multilayer thin-films [7], for instance, the oxide–nitride bi-layer structure proposed in [8] and the ONO (oxide–nitride–oxide) tri-layer structure proposed in [9]. These two approaches are aimed at reducing the net residual stresses instead of increasing the stiffness of the micromachined structure. However, the unwanted deformation of the micromachined structure caused by external loads still cannot be reduced. In addition, the applications of these approaches are limited by the available thin-film materials as well as the fabrication processes. Consequently, it is useful to increase the stiffness of the micromachined structure to improve the performance of various MEMS devices [10–12]. The processes used to fabricate thicker micromachined structures have been developed to increase the bending stiffness of the micromachined structure [13]. In this case, complicated fabrication processes as well as special equipment are required.

In the present study, the concept of increasing the bending stiffness of the micromachined beam using the rib-reinforced micromachined structures shown in figure 1 is proposed. This idea is investigated through experimental and analytical approaches. It is demonstrated that the bending stiffness of the proposed design is increased by changing the geometry of the cross section of the structures, whereas, the thickness of the structure remains unchanged. Therefore, the micromachined structure has less deformation no matter if it is under residual stresses or under external loads.

2. Analysis

A cantilever beam of uniform cross section along its length will be bent after being subjected to a pure bending moment M. The radius of curvature ρ of the beam is constant along the beam length, and can be represented as [14]

$$\rho = \frac{EI}{M} \qquad (1)$$

where E is the elastic modulus of the material and I is the moment of inertia of the cross section with respect to the centroidal axis. According to (1), the radius of curvature ρ of a beam due to M varies linearly with the moment of inertia I. The conventional micromachined beam with a rectangular cross section shown in figure 2(a) has a moment of inertia $I_0 = bh^3/12$, where b is the beam width and h is the beam thickness. Hence, to increase the film thickness h

0960-1317/00/010093+07$30.00 © 2000 IOP Publishing Ltd

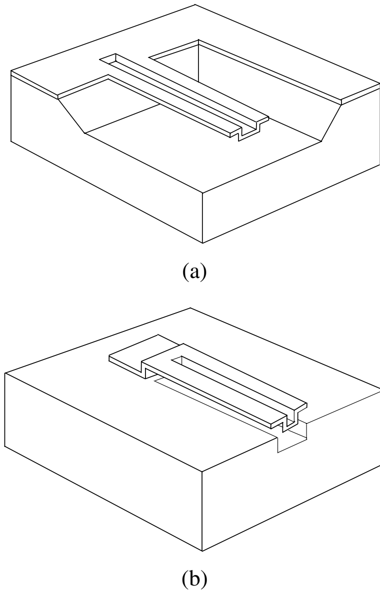

Figure 1. The schematic view of the proposed rib-reinforced micromachined beams: (a) the beam fabricated by bulk micromachining and (b) the beam fabricated by surface micromachining.

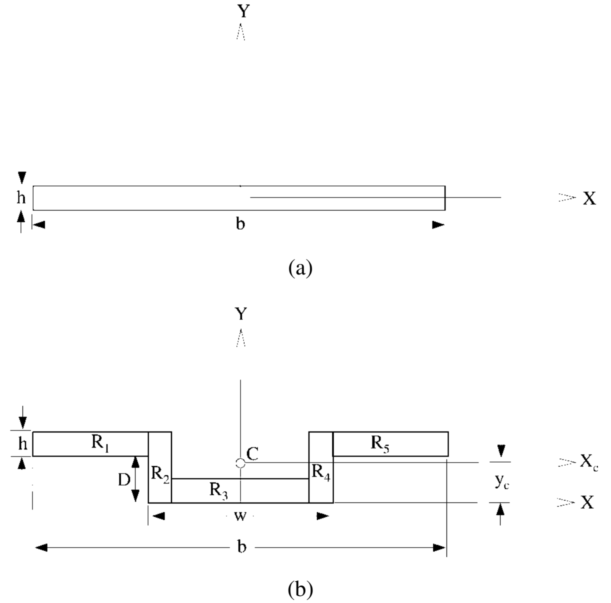

Figure 2. The cross section of (a) the conventional micromachined beam with a rectangular cross section and (b) the rib-reinforced micromachined beam.

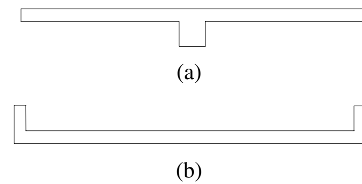

Figure 3. Two possible cross sections of the rib-reinforced micromachined beams: (a) the T-shaped cross section and (b) the U-shaped cross section.

is the only approach to increase the bending stiffness of the micromachined beam, when b is specified.

This work attempts to increase the moment of inertia of the beam by means of changing the shape of its cross section; thus, the bending stiffness of the micromachined beam is increased. In this study the structure is called the rib-reinforced beam. A typical cross section of the rib-reinforced cantilever is illustrated in figure 2(b). The cross section of the cantilever can be adjusted by changing the trench depth D and trench width w, as indicated in figure 2(b). The point C represents the centroid of the cross section. Consequently, the mechanical properties of the beam such as resonant frequencies and torsional stiffness will also be changed. To simplify the analytical model, it was assumed that the cross section of the cantilever has a uniform thickness h. The side walls of the trench were assumed to be perpendicular to each other, as indicated in figure 2(b). Furthermore, the stress concentration effect was neglected in the model.

2.1. Bending stiffness

The moment of inertia about the neutral axis X_c of the cross section in figure 2(b) is [14]

$$I' = \sum (I_i + A_i d_i^2) \tag{2}$$

where subscript i denotes the number of rectangular subregions inside the cross section. As shown in figure 2(b), the cross section was divided into five rectangles, R_1–R_5, thus $i = 5$. I_i and A_i represent the moment of inertia and the area of the R_i rectangle, respectively. The distance from the centroid of the R_i rectangle to the X_c axis is represented by d_i. The moment of inertia I_i of each rectangular subregion is $I_i = b_i h_i^3/12$. According to (2), the moment of inertia I' of the cross section shown in figure 2(b) can be adjusted by varying w and D. In other words, the bending stiffness of the proposed rib-reinforced micromachined cantilever can be increased without changing the film thickness h.

In general, the rib-reinforced beam has a hat-shaped cross section with different w and D as illustrated in figure 2(b). As one of the limiting case, the cross section illustrated in figure 3(a) becomes T-shaped when $w = 2h$. The cross section becomes U-shaped when $w = b$, as shown in figure 3(b). If the trench depth D is zero, then the cross section of the micromachined beam becomes rectangular. The variation of the bending stiffness with the parameters w and D of the proposed cross section design was obtained from equation (2). As shown in figure 4, the curves reveal the variation of I'/I_0 with D and w when the beam width $b = 30$ μm and the film thickness $h = 1$ μm. According to the results shown in figure 4, even a shallow and narrow trench may still significantly increase the bending stiffness of the beam. For instance, the bending stiffness of the cantilever with a $D = 1$ μm and $w = 3$ μm cross section is 2.16 times greater than that with a rectangular cross section. Also obtained from figure 4 is that I' is significantly increased when the depth D of the trench is increased, and I' has a maximum when $w = b/2$.

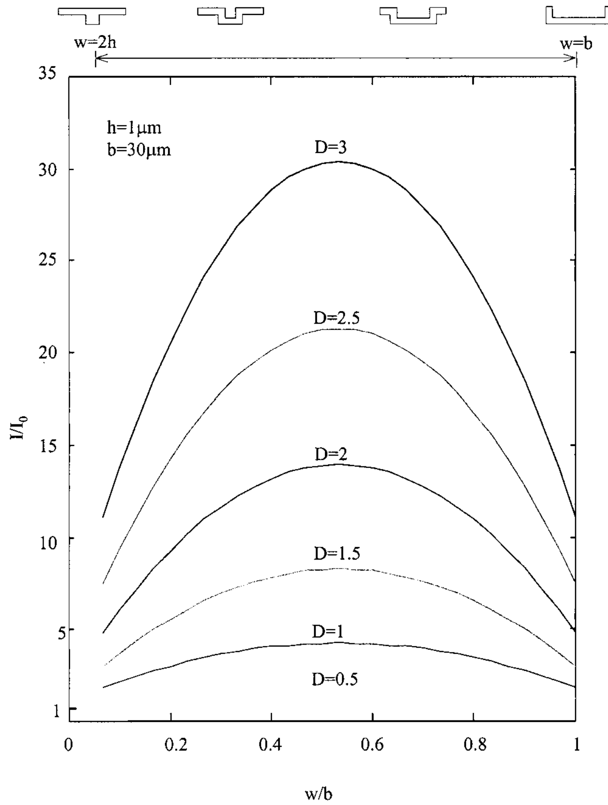

Figure 4. The variation of the bending stiffness with the trench depth D and width w of the rib-reinforced micromachined beams.

2.2. Torsional stiffness

The cross section of the micromachined beam is considered as a thin-walled open section. Hence, the torsional stiffness K_t for the proposed design can be represented as [15]

$$K_t = G \sum \frac{1}{3} b_i h^3 \tag{3}$$

where subscript i denotes the number of rectangular subregions inside the cross section, G is the shear modulus of the thin-film material and b_i is the length of each rectangular subregion. The torsional stiffness for the beam with a rectangular cross section is $K_{t0} = Gbh^3/3$, for the beam with T-shaped cross section it is $K_{tT} = G(b + D)h^3/3$, and for the beam with U-shaped and hat-shaped cross sections it is $K_{tH} = G(b + 2D)h^3/3$.

As shown in figure 4, the stiffness of the beam with the hat-shaped cross section is twice as much as that with a rectangular cross section when $D = 1$ μm, $w = 3$ μm and $b = 30$ μm. In this case, the torsional stiffness K_{t0} and K_{tH} differed by only 6.7%. On the other hand, if the bending stiffness is increased through an increase of the thin-film thickness h, the torsional stiffness will also be increased, by twice as much. In short, the rib-reinforced beam provides the possibility of increasing the bending stiffness of the beam while its torsional stiffness remains unchanged.

3. Experiment and results

In order to demonstrate the concept proposed in the present study, the micromachined cantilevers with conventional

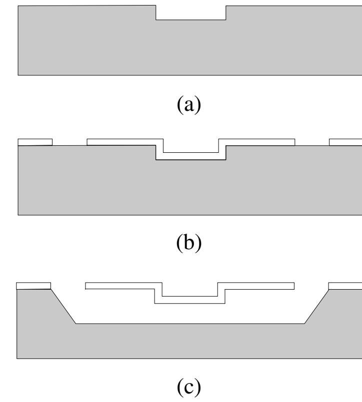

Figure 5. The fabrication processes for a rib-reinforced micromachined beam.

rectangular and rib-reinforced hat-shaped cross sections were fabricated. The deflection configurations of the cantilevers were measured using optical interferometry. According to the deflection profile, the radius of curvature as well as the bending stiffness of the micromachined cantilevers were determined.

3.1. Fabrication processes

In application of this technique, the rib-reinforced cantilevers with different h, w and D, were fabricated through standard bulk micromachining. The major fabrication processes are shown in figure 5. As shown in figure 5(a), the width w of the trench was defined by the first mask and then the depth D of the trench was determined by the reactive ion etching process. After the thin-film material was deposited onto the substrate, the width d and the length L of the cantilevers were defined by the second mask, as shows in figure 5(b). Finally, the rib-reinforced cantilevers were suspended as shown in figure 5(c) after the substrate was undercut by wet anisotropic etching. The limitation of the trench depth D has to be taken into consideration in order to recover the step coverage effect during thin-film deposition.

The SEM photograph of eight, typical, rib-reinforced cantilever beams, 0.9 μm thick, 30 μm wide, and 50–250 μm long is shown in figure 6. The cross section of a typical hat-shaped beam with a 12 μm wide and 0.9 μm deep trench is shown in figure 7. The beams shown in figures 6 and 7 were made of plasma enhanced chemical vapour deposition (PECVD) Si_xN_y; in addition, the 1.5 μm thick low pressure chemical vapour deposition (LPCVD) Si_xN_y beams were available in the experiment. In order to compare the difference of the bending stiffness between the conventional beam and the rib-reinforced beam, the cantilevers with a rectangular cross section were also fabricated, as shown in figure 8(a). The beams shown in figure 8(b) have the same thickness as well as length as the rectangular beams in figure 8(a). Compared with the rib-reinforced beams shown in figure 8(b), the deflection of the conventional beams was significant; even being visible in figure 8(a).

3.2. Measurement and results

The residual gradient stress will introduce an equivalent bending moment M to the micromachined structures [1].

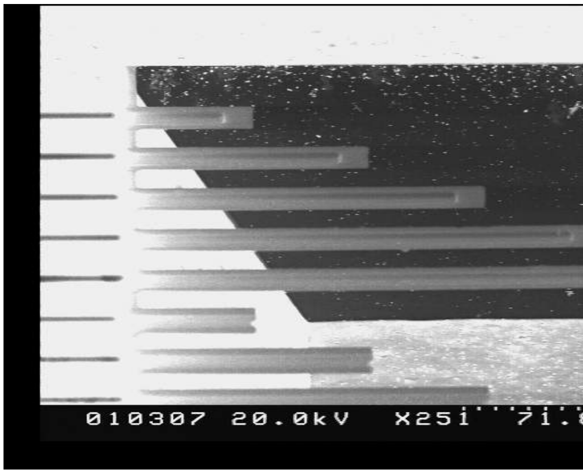

Figure 6. A SEM photograph of the rib-reinforced micromachined beams: 0.9 μm thick, 30 μm wide and 50–250 μm long. The trench is 15 μm wide and 0.9 μm deep.

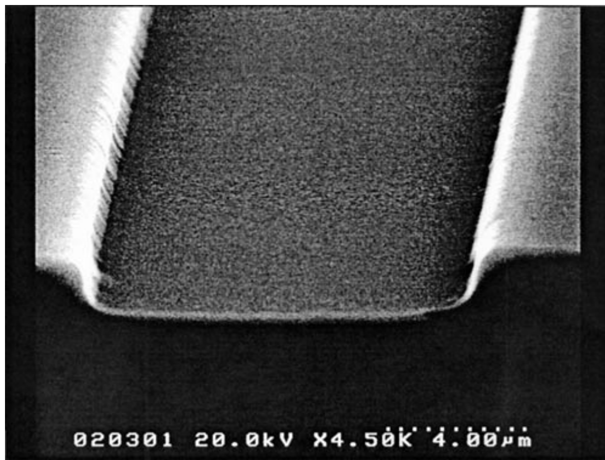

Figure 7. A SEM photograph of the cross section of a rib-reinforced beam with a 15 μm wide and 0.9 μm deep trench.

According to (1), the cantilever beam will be bent by M with a constant radius of curvature ρ along the beam length. In this study, the gradient residual stress of the thin film was exploited to bend the micromachined cantilevers; thus, the bending stiffness of the cantilevers were determined by ρ.

In application of this technique, the deflection configurations of the 0.9 μm thick PECVD Si_xN_y cantilevers were measured first. A non-contact interferometric profilometry system was used to characterize the deflected profile of the beams in this experiment. Typical measured profiles of two cantilevers are shown in figure 9. The points A and B indicated in figure 9 represents the fixed end and the free end of the beam, respectively. In other words, the measured profile ranging from $x = 0$ to 50 μm shows the region where the thin-film is still bonded to the substrate. The measured profile ranging from $x = 50$ to 140 μm shows the deformation profile of the cantilever. Hence, the radius of curvature ρ of the beam was obtained. Since the deflection of the beam with a rectangular cross section is too large to be measured when $x > 130$ μm, the profile at this region is not available in figure 9(a).

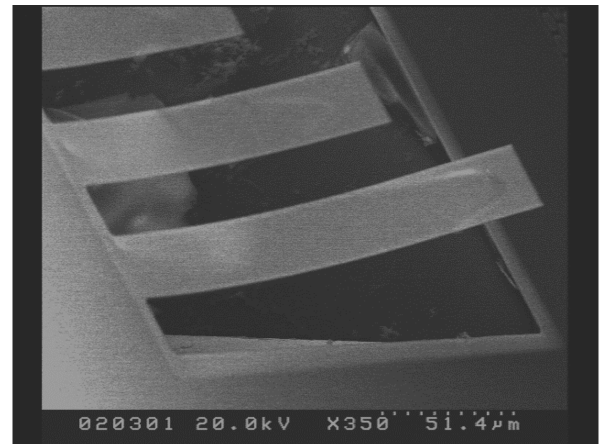

(a)

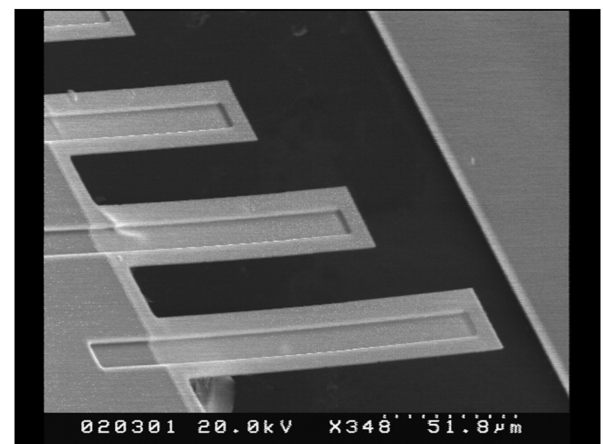

(b)

Figure 8. A SEM photographs of the deflection of (a) conventional beams, and (b) rib-reinforced beams, when under the same stress condition.

The deflection profile shown in figure 9(a) is a 100 μm long and 30 μm wide cantilever with a rectangular cross section. The radius of curvature of the deformed beam is $\rho_0 = 490$ μm. The deflection profile shown in figure 9(b) is a 100 μm long and 30 μm wide cantilever with a hat-shaped cross section. The trench of this hat-shaped cross section is $w = 12$ μm and $D = 0.9$ μm. The radius of curvature of the deformed beam is $\rho = 2890$ μm. It is evident that the bending stiffness of a rib-reinforced beam is 5.93 times greater than that of a conventional beam. According to the experimental results, it is demonstrated that the proposed design can remarkably increase the bending stiffness of the micromachined structures.

As a second example, the 1.5 μm thick LPCVD Si_xN_y cantilevers were characterized. The deflection profile shown in figure 10(a) is a 150 μm long and 30 μm wide cantilever with a rectangular cross section. The radius of curvature of the deformed beam is $\rho_0 = -10\,320$ μm. The negative sign means that the beam was bent downwards. Therefore, the bending moment induced by the gradient residual stress of the LPCVD Si_xN_y film has an opposite direction to that of the PECVD Si_xN_y film. The deflection profile shown in figure 10(b) is a 150 μm long and 30 μm wide cantilever

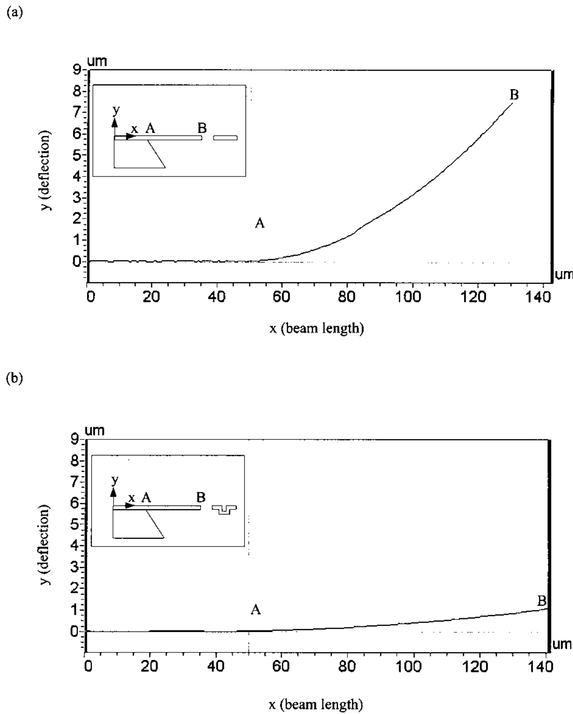

Figure 9. The measured deflection profile of 0.9 μm thick LPCVD Si_xN_y beams, (a) a conventional beam and (b) a rib-reinforced beam with a 15 μm wide and 0.9 μm deep trench.

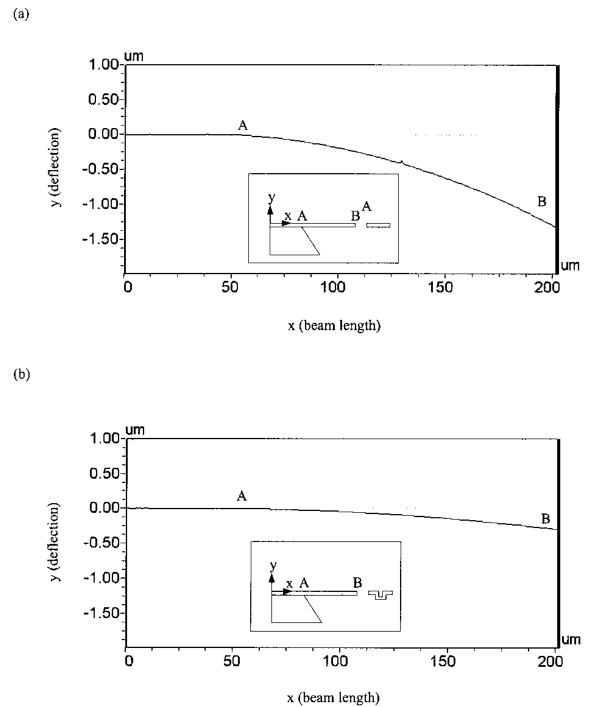

Figure 10. The measured deflection profile of 1.5 μm thick LPCVD Si_xN_y beams, (a) a conventional beams and (b) a rib-reinforced beam with a 15 μm wide and 0.9 μm deep trench.

with a hat-shaped cross section. The trench of this hat-shaped cross section is $w = 13$ μm and $D = 1.3$ μm. The radius of curvature of the deformed beam is $\rho = -46\,130$ μm. It is evident that the bending stiffness of a rib-reinforced beam is 4.47 times greater than that of a conventional beam.

4. Application

In application of the rib-reinforced structure, the lever mechanism illustrated in figure 11 is designed and fabricated. The lever mechanism is exploited to amplify the displacement of a MEMS device in the out-of-plane direction. Thus, the out-of-plane motion for MEMS devices will not be limited by the structural design or the driving mechanism. The lever mechanism in figure 11(a) contains one arm with length L $(= L_1 + L_2)$ and a pivot. The lever arm is assumed to be a rigid body for the ideal case. In figure 11(b), the torsion bar is used as the pivot of the lever mechanism. The amplification ratio of the travelling distance between the output end x_2 and input end x_1 becomes L_2/L_1. The design can be extended to the multiple-lever-arms mechanism shown in figure 12. The amplification ratio of the travelling distance between the output end x_4 and input end x_1 becomes L_2L_4/L_1L_3.

The amplification ratio of the displacement is significantly decreased if the stiffness of the lever arm is small. This is mainly due to the bending deformation of the lever arms. For instance, the finite-element model established in figure 13(a) simulates a 2 μm thick and 300 μm long LPCVP Si_xNi_y lever arm. Analysis shows that its magnification ratio is only 57% of that obtained from the rigid lever arm. The lever arm with rib-reinforced

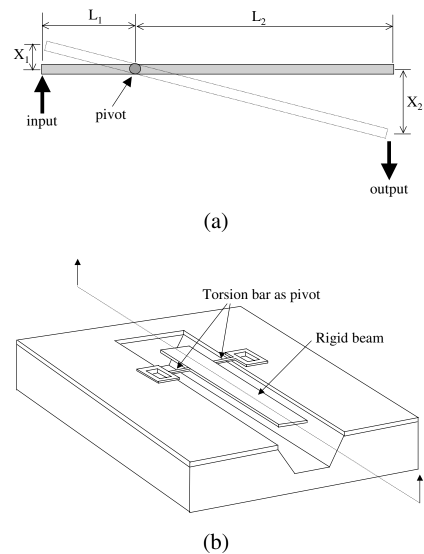

Figure 11. The (a) side view and (b) isometric view of a single-arm lever mechanism.

cross section is used to increase its bending stiffness. The bending stiffness can thus be adjusted by changing the parameters h, w and D, as indicated in figure 2. As shown in figure 13(b), the amplification ratio of the rib-reinforced lever is 1.6 times larger than that of the conventional lever. For the two-arm lever mechanism shown in figure 11(b), an even higher ratio is obtained; the amplification ratio of the rib-reinforced lever is 10 times larger than that of the conventional two-arm lever. In short, the bending stiffness of the lever arm can be significantly increased, leading to

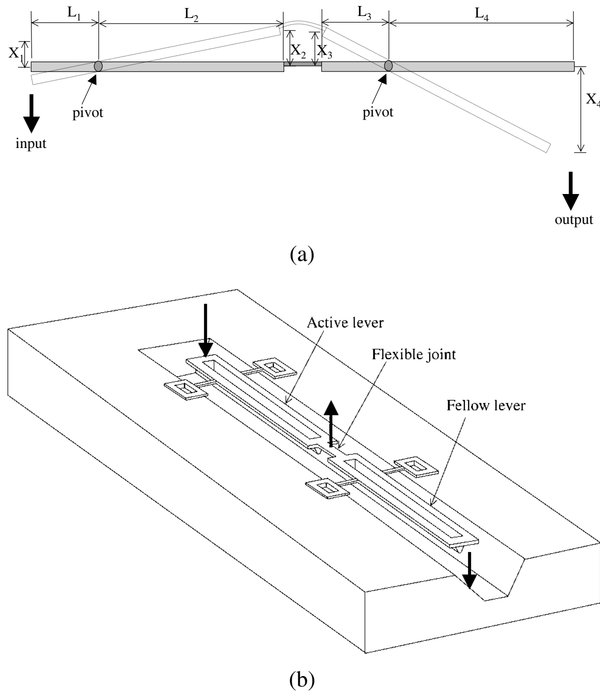

Figure 12. The (a) side view and (b) isometric view of a two-arms lever mechanism.

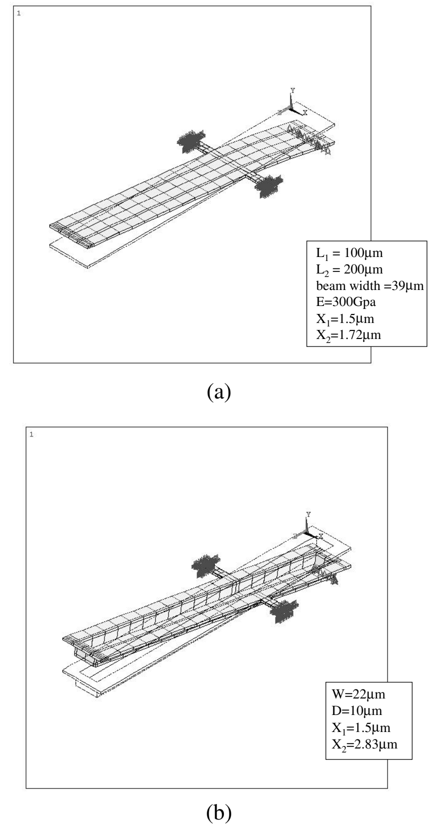

Figure 13. Finite-element models of (a) a conventional beam and (b) a rib-reinforced beam single-arm lever mechanisms.

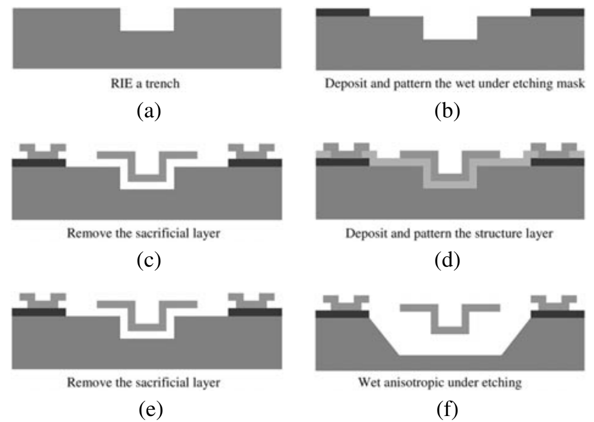

Figure 14. The fabrication processes for the micromachined lever mechanism.

an improved performance of the lever mechanism. The lever mechanism with the rib-reinforced arms was fabricated following the similar steps shown in figure 14. A SEM photograph of a two-arm lever mechanism is shown in figure 15.

5. Discussion and conclusion

According to the analytical results, the bending stiffness of a rib-reinforced PECVD Si_xN_y cantilever is 4.05 times greater than that of a conventional beam. However, the I'/I_0 of PECVD Si_xN_y cantilevers measured in section 3 is only 1.46 times greater than that analysed. The I'/I_0 of LPCVD Si_xN_y cantilevers measured in section 3 is only 1.38 times greater than that analysed. It is believed that the mismatch between the measured and analytical results is mainly due to the deviation of the thin-film thickness. The moment of inertia I_0 varies cubically with the thin-film thickness h. Whereas, the moment of inertia I', as described in (2), varies cubically with film thickness h for the first term and varies linearly with h for the second term. Consequently, the bending stiffness of the rectangular cross sectional beam is more sensitive to the variation of h. In this case, the I'/I_0 will be increased when the film thickness is decreased. The ratio of I'/I_0 is greater than the predicted value since the film is thinner than expected after bulk etching. Additional experimental work will still be required to fully understand the reason for the deviation of the I'/I_0.

In this research, the idea of increasing the bending stiffness of micromachined structures has been demonstrated through analytical and experimental approaches. The fabrication processes required for the rib-reinforced structures are compatible with standard bulk micromachining processes. The primary contribution of the proposed design is that it can remarkably increase the bending stiffness of the micromachined structure without increasing the thickness of the films. The bending stiffness of the proposed design can be adjusted by changing the dimensions, such as width w and depth D, of the trench. Hence, the design of the micromachined structure becomes more flexible and the bending stiffness of the structures is no longer limited to the thickness of the thin films. In figure 15, the micromachined lever mechanism that contains the rib-reinforced arm is designed, fabricated and analysed. A flatter micromachined component such as the mirror plate in [12] is also available and the deformation of the micromachined

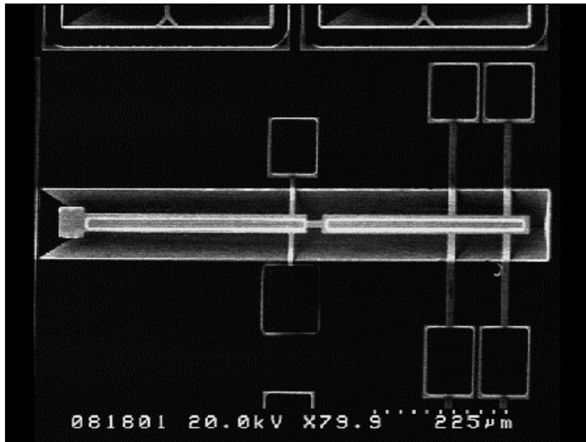

Figure 15. A SEM photograph of the two-arms lever mechanism.

beam led by the deposition of an additional film is prevented. In addition, the performance of the torsional mirror in [3] can be improved since its torsional stiffness remains unchanged when its bending stiffness is increased using the rib-reinforced design.

Acknowledgments

This material is based (in part) upon work supported by the National Science Council (Taiwan) under Grant NSC 88-2218-E007-004. The author would like to express his appreciation to the Electrical Engineering Department of National Tsing Hua University (Taiwan), Semiconductor Center of National Chiao Tung University (Taiwan), and National Nano Device Laboratories (Taiwan) in providing fabrication facilities.

References

[1] Fang W and Wickert J A 1996 Determining mean and gradient residual stress in thin-films using micromachined cantilevers *J. Micromech. Microeng.* **6** 301–9

[2] Guckel H, Burns D, Rutigliano C, Lovell E and Choi B 1992 Diagnostic microstructures for the measurement of intrinsic strain in thin-films *J. Micromech. Microeng.* **2** 86–95

[3] Hsieh J and Fang W 1998 Fabrication of micro torsional actuator using surface plus bulk micromachining processes *SPIE Micromachining Microfabrication* **3514** 368–76

[4] Conant R A, Hagelin P M, Krishnamoorthy U, Solgaard O, Lau K Y and Muller R S 1999 A raster-scanning full-motion video display using polysilicon micromachined mirror *Transducers'99 (Sendai, Japan, June 1999)* pp 376–9

[5] Claassen W A P, Valkenburg W G J N, Willemsen M F C and van de Wijgert W M 1985 Influence of deposition temperature, gas pressure, gas phase composition, and RF frequency on composition and mechanical stress of plasma silicon nitride layers *J. Electrochem. Soc.* **132** 893–8

[6] Zhang X, Zhang T Y, Wong M and Zohar Y 1998 Residual-stress relaxation in polysilicon thin-films by high-temperature rapid thermal annealing *Sensors Actuators* A **64** 109–15

[7] Ried R P, Kim E S, Hong D M and Muller R S 1992 Residual-stress compensation in clamped-clamped micromachined plates *Micromechanical Systems ASME Winter Annul Meeting (Anaheim, CA, November 1992)* pp 23–32

[8] Chou B C S, Shie J-S and Chen C-N 1997 Fabrication of low-stress dielectric thin-film for microsensor applications *IEEE Electron Device Lett.* **18** 599–601

[9] Volklein F 1990 Thermal conductivity and diffusivity of a thin-film SiO_2–Si_3N_4 sandwich system *Thin Solid Films* **188** 27–33

[10] Jerman J H, Clift D J and Mallinson S R 1991 A miniature Fabry-Perot interferometer with a corrugated silicon diaphragms support *Sensors Actuators* A **29** 151–8

[11] Lee S S, Ried R P and Write R M 1996 Piezoelectric cantilever microphone and microspeaker *J. Microelectromech. Syst.* **5** 238–42

[12] Hwang K-H, Koo W-K and Kim S-G 1998 High brightness projection display system based on the thin-film actuated mirror array (TFAMA) *SPIE Micromachining Microfabrication* **3513** 171–80

[13] MacDonald N C 1996 SCREAM microelectromechanical systems *Microelectron. Eng.* **32** 49–73

[14] Beer F P and Johnston E R Jr 1992 *Mechanics of Materials* (New York: McGraw-Hill)

[15] Cook R D and Young W C 1985 *Advanced Mechanics of Materials* (New York: Macmillan)